

Hadronic Interactions at Ultra High Energies with Extensive Air Showers

Lorenzo Cazon*

Instituto Galego de Física de Altas Enerxías (IGFAE), University of Santiago de Compostela, Spain

E-mail: lorenzo.cazon@usc.es

This article reviews the use of observations performed with extensive air showers to probe hadronic interactions at high energy. It provides an overview of new studies exploring the connection between the dynamics of air showers and multiparticle production and how this knowledge can be translated into constraints on high-energy hadronic models. Additionally, it looks at direct measurements complementary to and beyond the reach of accelerator experiments.

*27th European Cosmic Ray Symposium -ECRS2022-
July - August, 2022
The Netherlands*

*Speaker.

1. Introduction

At energies higher than 10^{15} eV, Extensive Air Showers (EAS) are used to detect Cosmic Rays (CR). These EAS contain data about the primary CR particle, such as its energy, mass number, and direction of arrival. Additionally, the EAS also contain information about particle interactions which happen in phase-space regions not accessible to accelerators. A centre-of-mass energy of around 14 TeV corresponds to a laboratory energy of 10^{17} eV, which is the threshold for using the name of Ultra High Energy Cosmic Rays (UHECR). UHECR can reach energies up to 10^{20} eV, which is around 30 times the center of mass energy reached at the Large Hadron Collider (LHC).

The extrapolation of our knowledge from particle accelerator measurements to the highest and most extreme energies has an associated uncertainty that grows as we move away from the tested regions. The interpretation of the UHECR mass in terms of EAS observables inherits the model uncertainties as one of the main contributions to the systematic uncertainties. In this sense, primary mass and hadronic interactions uncertainties are difficult to untangle from an experimental point of view.

Testing particle physics and extracting mass composition mostly rely on comparisons of full EAS simulations with data taken by EAS experiments. These simulations include all interactions occurring within the air-shower at high and low energies. The secondaries arising after the first interaction undergo successive particle reactions creating again new particles, and making EAS achieve macroscopic size. As a consequence, most details of the multi-particle production of the first interaction are hidden within the vastness of all particles of the cascade. A group of n shower observables might still be sensitive to changes in primary mass and hadronic physics. This can be used to define a point on the n -dimensional space. Given that primary mass is unknown, EAS simulations must be performed assuming all possibilities of mass compositions mixes, reaching across an extended region on the n -dimensional space of observables. On the contrary, data will be an n -dimensional single point. A direct comparison of data with the phase space of simulations performed with a high energy interaction model allows to exclude particle physics and / or mass composition scenarios.

Two ways are used to measure EAS: one involves detecting the electromagnetic radiation released when cascading charged particles (mainly electrons) interact with air molecules and the geomagnetic field (UV-light: Fluorescence light, Cherenkov, MHz radio: Geosynchrotron, Cherenkov), and the other entails capturing the particles that make it to the ground (mainly electrons, photons and muons).

2. Air Shower Physics

Following the first interaction between a UHECR and an atmospheric nucleus, the majority of the energy (around 80%) is converted into secondary mesons and baryons which go on to interact and create a so-called hadronic cascade. Figure 1 illustrates the average energy distribution among different particle groups in interactions involving protons, pions and kaons at 10^{19} eV, as simulated by various models. The pion sector includes the decay $\rho^0 \rightarrow \pi^+ \pi^-$, and the baryon sector includes protons, neutrons, Λ particles and their antiparticles. As the average energy per meson decreases, the likelihood of the mesons decaying instead of interacting increases, and this is known as the

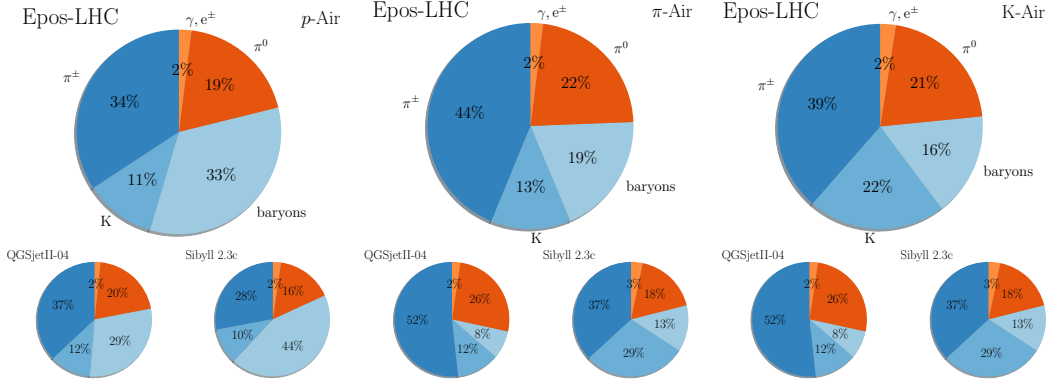


Figure 1: Average share of energy among different groups of particles in p -Air (left), π -Air (centre), and K -Air (right) interaction at 10^{19} eV, simulated with different models, as labelled. Numbers are in percent. Particles contributing to the electromagnetic component are shown in shades of red, particles in the hadronic component are shown in shades of blue. The contributions to the π^\pm sector include the decay $\rho^0 \rightarrow \pi^+ \pi^-$. The baryon sector includes p, n, Λ and their antiparticles.

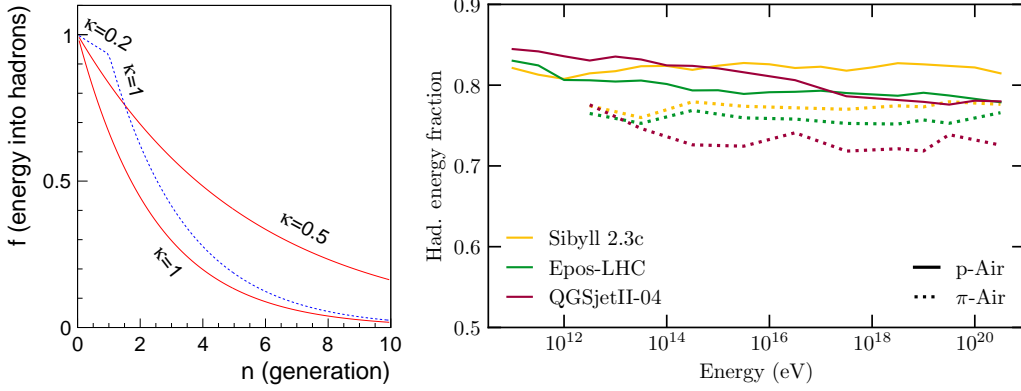


Figure 2: Left: energy fraction evolution with generation n , taken from a Heiler-Matthews model with different κ parameters, taken from [3]. Right: Hadronic energy fraction f as a function of energy, for p -Air and π -Air interactions simulated with several models.

critical energy. The critical energy for pions, kaons and K_L^0 and K_S^0 particles is approximately 100 GeV, 1000 GeV, 200 GeV and 30 TeV respectively. Muons mostly come from pion decay and some of the kaon decay channels. Muons can be considered main messengers from the hadronic cascade.

The EM cascade is formed by the decay of neutral pions π^0 into photons, which then undergo pair production and bremsstrahlung to create more photons and electrons. Approximately 25% of the hadronic cascade's energy is transferred to the EM cascade (through π^0) right from the very first interaction. The evolution of the total amount of energy carried by particles in the EM and hadronic components can be seen in Figure 2 (right).

The features of hadronic showers can be roughly estimated using the pionic Heitler-Matthews

model [1], which states that in each generation¹ of particles, two thirds of them will be charged pions and one third will be neutral pions. The energy fraction of charged pions to the total shower energy E_0 in each generation is

$$\frac{\sum E_\pi}{E_0} = f^n = (1 - f_{\text{EM}})^n \quad (2.1)$$

The energy carried by charged pions in each generation is decreased by a factor of f . The model can be further refined: if a leading baryon takes $(1 - \kappa)E_0$, then the energy flowing to the EM cascade would be lessened by $f_{\text{EM}} = 1/3\kappa$, as explained in [1]. Additionally, other processes could potentially reduce the energy that goes to the EM channel, such as increased kaon production [2].

The evolution of the energy distribution between both cascades is illustrated in Figure 2 (left) for a pure pionic cascade ($\kappa = 1$) and a more realistic case ($\kappa = 0.5$, $f_{\text{EM}} = 0.17$)[3]. Initially, all the energy is in the hadronic sector. However, after three generations, most of the energy has been transferred to the EM cascade, at which point the hadronic and EM processes can be considered decoupled. The number of muons arising from the hadronic cascade is roughly $N_\mu = E_0 f^c / \xi_{\text{crit}}^{\pi^\mp}$, where all successive interactions down to the critical generation $n = c$ have contributed. In contrast, the EM cascade is dominated by the most energetic π^0 contributions.

2.1 Electromagnetic and hadronic Shower

In addition to the direct muon component and the pure electromagnetic (EM) component arising from high-energy π^0 decays, other contributions have been identified [4, 5]. These are: the muons created from photopion interactions connected to the EM cascade, the EM component that stems from muon decay (known as the muon halo) which is proportional to the hadronic shower, and finally the EM radiation from low energy π^0 decays, a small contribution that is related to the hadronic cascade.

The research of showers initiated by photons and electrons is well-documented in literature: the longitudinal development of the number of electrons is described by a Greisen profile [6]. For a hadron-induced shower, each π^0 decay creates its own contribution to the electromagnetic component, forming a Gaisser-Hillas profile [7]. Several studies, such as [8, 9, 10, 11], have found that the electron energy spectra, lateral distributions, and angular distributions can be universally expressed in terms of shower age and Moliere radius. This concept of universality of showers is especially important in experiments, as it allows the fundamental properties of the shower to be determined by fitting universal templates to the observed particle distributions.

In [12], it was determined that the muon component of air showers can be accurately described using the equation

$$\frac{d^3N}{dX dE_i dcp_t} = \mathcal{N}_\mu f(X - \mathcal{X}_{\text{max}}^\mu, E_i, cp_t) \quad (2.2)$$

where \mathcal{N}_μ is the total number of muons produced in the shower, X is the slant depth, $\mathcal{X}_{\text{max}}^\mu$ is the depth where the rate of muon production reaches a maximum, E_i is the energy of the muons at production, and cp_t is the transverse momentum with respect to the shower axis. In [12] it was

¹Generation $n = 1$ for particles coming from the initial interaction, generation $n = 2$ for particles coming from the interaction of those of generation $n = 1$, and so on so forth.

demonstrated that this distribution can be used to propagate muons to obtain any distribution at ground: lateral distribution function, *apparent* Muon Production Depth (MPD) distribution and its maximum X_{\max}^{μ} , arrival time distribution, energy spectrum, *et cetera*. The 3-dimensional distribution of Eq. 2.2 is directly inherited from the hadronic cascade. The cp_T -distribution and to a lesser extent the *total/true* MPD distribution are universal across primaries and models when referred to the maximum $X' \equiv X - X_{\max}^{\mu}$, whereas the E_i -distribution shows sizeable differences across models and primaries [12, 13]. Figure 3 shows 3 of these distributions for the post-LHC hadronic models.

Pions and kaons in EAS typically interact several times ($\mathcal{O}(10)$) before they decay and produce muons. In [13] it was shown that the final transverse momentum of these cascading mesons is mostly determined by the transverse momentum obtained in the last interaction i that produced the decaying pion (meson),

The angle γ of the muons exiting the shower axis is determined by the energy and transverse momentum of the parent pion. The perpendicular distance to the shower axis before pion decay is $r_{\pi} = cp_{\pi}c\tau_0/(m_{\pi}c^2)$, where $c\tau = E_i/(m_{\pi}c^2)c\tau_0$ is the pion decay time. The transverse momentum of the muons is distributed according to $dN/dp_T = (p_T/Q^2)\exp(-p_T/Q)$, with $cQ \sim 0.2$ GeV. This means that 60% of the muons are produced within $r_{\pi} < 22$ m - much smaller than the typical lateral distances of observation in experiments. Consequently, it can usually be assumed that the muons are produced in the shower axis.

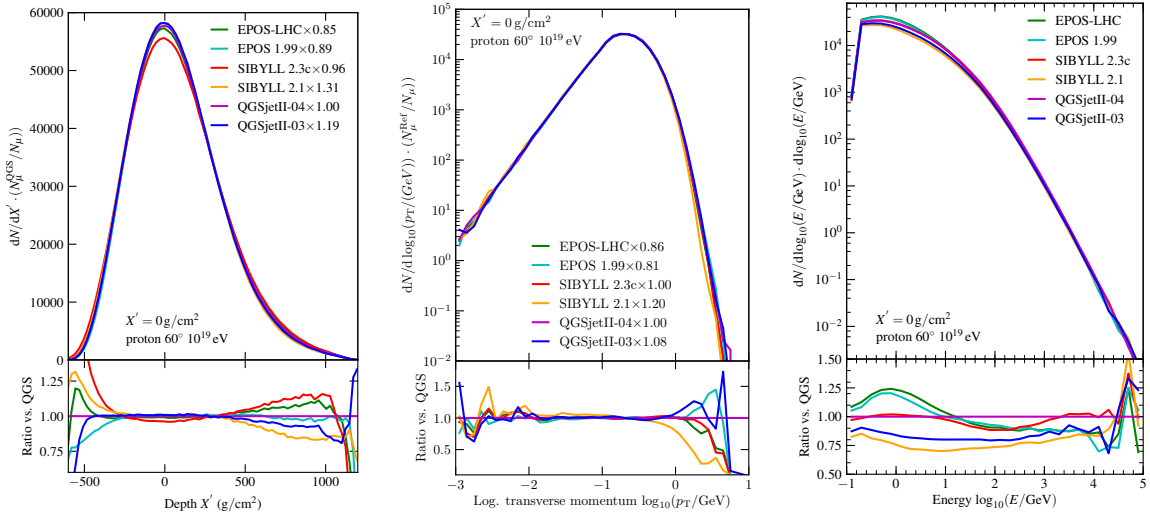


Figure 3: *Total/true* Muon Production Depth distribution (left), transverse momentum distribution at production (centre), muon energy distribution at production (right), for proton showers simulated at 10^{19} eV, taken from [13].

In [13] it was discussed to what degree the distribution in the transverse momentum, the depth of production, and the energy at production of the muons are universal when referred to the depth where the muon production reaches its maximum, i.e. by how much the shape of these three distributions varies with zenith angle, primary particle, primary energy, and hadronic interaction model. It was shown that the transverse-momentum and production-depth distributions are fairly universal with a maximal variation of $4\text{MeV}/c$ (2% relative variation) in case of the p_T spectrum and $13\text{g}/\text{cm}^2$ (5% relative variation) in case of the MPD. The most significant deviations from uni-

versality are seen in the energy spectrum between primaries which varies by 50MeV to 80MeV (7% to 9%). Therefore, the only significant differences across models arise in the muon energy spectrum, particularly in the high-energy tails.

2.2 High Energy Hadronic Models

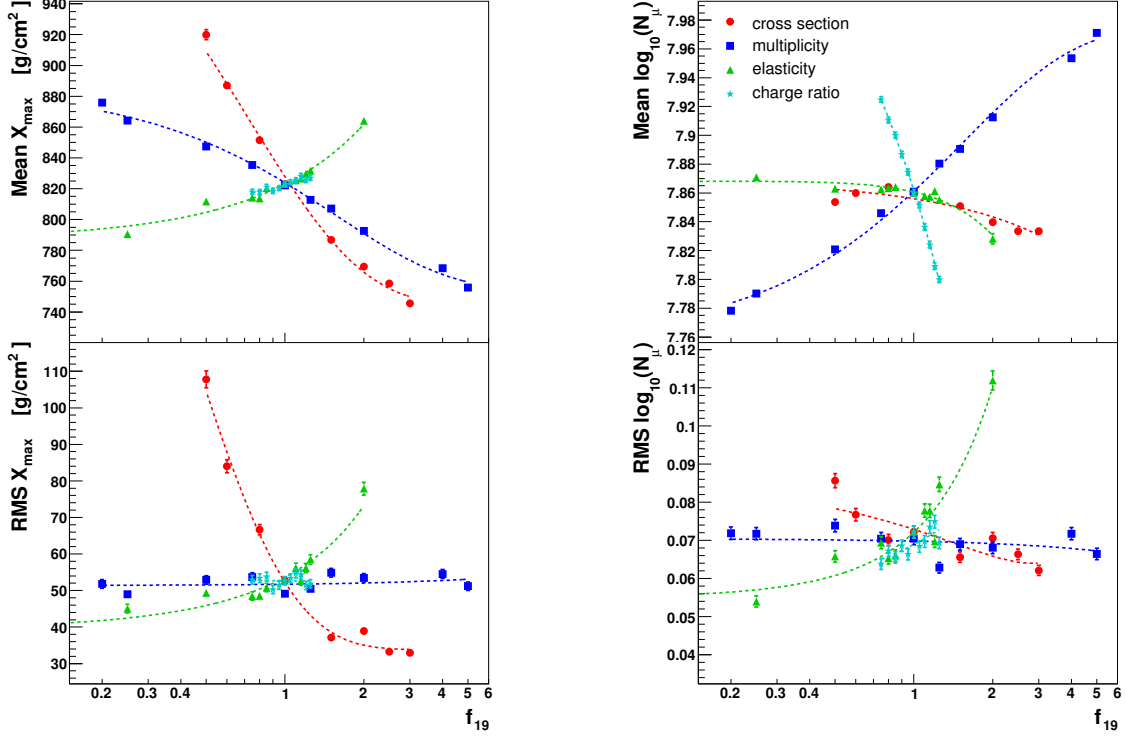


Figure 4: Impact of a modified extrapolation of hadronic interaction features on depth of shower maximum X_{\max} (left) and the number of muons N_{μ} (right) as a function of the scaling hadronic parameter f_{19} for a simulated proton shower at $10^{19.5}$ eV with SIBYLL-2.1. (Taken from [14].)

The effects of changing the hadronic interaction parameters on several air shower observables were considered in [14]. The parameters looked at were the p-Air cross-section, total multiplicity, elasticity (fraction of energy taken by the leading particle) and charge-ratio (a proxy for f_{EM}). The model utilized a continuous and gradual evolution of hadronic particle production from 10^{15} eV to high energy, and f_{19} as the scaling factor at 10^{19} eV. Figure 4, left-bottom panel, shows the effects on the fluctuations of the EM component in the longitudinal development ($RMS(X_{\max})$), which are mainly related to the cross section and to a lesser extent, the elasticity. The muon number (right, upper panel) can be increased by either raising the total multiplicity or decreasing the charge-ratio.

In terms of what experiments can measure, the central pseudorapidities are the most accessible region, as they contain the highest rapidity-density of produced particles. However, the forward region is what carries the most energy after the collisions, and is where the cascading process and the creation of new particles in the EAS occurs. Figure 5 displays simulated densities of prompt

particles (solid lines) in high-energy p-p, p-Pb, and p-O collisions along with the estimated number of muons produced by the secondaries if they were propagated through the atmosphere, assuming $N_\mu \propto E_{lab}^{0.93}$, where E_{lab} is the energy of the secondaries in the boosted system. In [15], a variety of forward detectors to study the energy spectra of forward particles which has a direct effect on air shower development are reviewed.

We focus in three hadronic interaction models, which are commonly used to simulate EAS, and were updated to take into account LHC data at 7 TeV: QGSJETII-03 [16] updated into QGSJETII-04 [17, 18], EPOS 1.99 [19] updated to EPOS-LHC [20], and SIBYLL-2.1 [21] updated to SIBYLL-2.3 [22] and SIBYLL-2.3c [23].

The inelastic cross section plays an important role in determining the depth of the initial interaction, X_0 , as well as the rate of interactions of secondary particles. This is demonstrated by Figure 4 in terms of the distribution of X_{max} . The p-p cross section has been accurately modelled up to the energy of the Large Hadron Collider, and the extrapolations from this point appear to be similar between models [25]. However, the extrapolations of the p-air and π -air inelastic cross-sections, which are more relevant for π -air interactions (which are the most common in shower formation), are not as consistent, as shown in Figure 6. Differences are also seen in the average multiplicity (Figure 6, right) at the highest energies. Therefore, the extrapolation to the highest energies in nuclear and pion interactions is still uncertain due to the lack of data on light ions at high energy.

Collider experiments do not directly constrain the elasticity, however, the extrapolations of p-air and π -air interactions are visible in Figure 7 (left) and entail a wide range of models. The right side of Figure 7 presents the rapidity gap cross-section which has a discrepancy between models and data. Large gaps are caused by single diffraction events and the elasticity and gap distributions illustrate the substantial ambiguities when modelling diffractive events. Figure 8 displays results for pPb collisions as recently published by CMS [26], showing a large discrepancy with respect to models.

Figure 9 displays the energy fraction of anti-protons at 158 GeV/c and 350 GeV/c (left) and ρ^0 at 158 GeV/c (right) as measured by the NA61/SHINE experiment in π^- -C interactions ([27, 28] and [29] respectively). Comparing the results to model predictions reveals discrepancies at low energies.

It is not easy to translate the results of p-p and p-Pb collisions to other nuclear targets. A reliable theory that can accurately predict the modifications of p-Air interactions has yet to be created. Investigations of p-O collisions at the LHC utilizing both heavy-ion and proton beams have been proposed in [30] and [31].

3. Experimental Observables

After the first report in 2000 by the HiRes/MIA collaboration about a muon deficit in simulations (*aka*, muon excess in data) between 10^{17} to 10^{18} eV [32], many more experiments have contributed with measurements. NEVOD-DECOR [33, 34] observed a muon deficit in simulations starting around 10^{18} eV as did the SUGAR array [35]. The Pierre Auger Observatory [36, 37, 38] and Telescope Array [39] reported a muon deficit with respect to the latest models in the energy range around and above 10^{19} eV. On the other hand, KASCADE-Grande [40] and EAS-MSU [41] reported no discrepancy around 10^{17} eV in the muon number. A comprehensive collection of muon

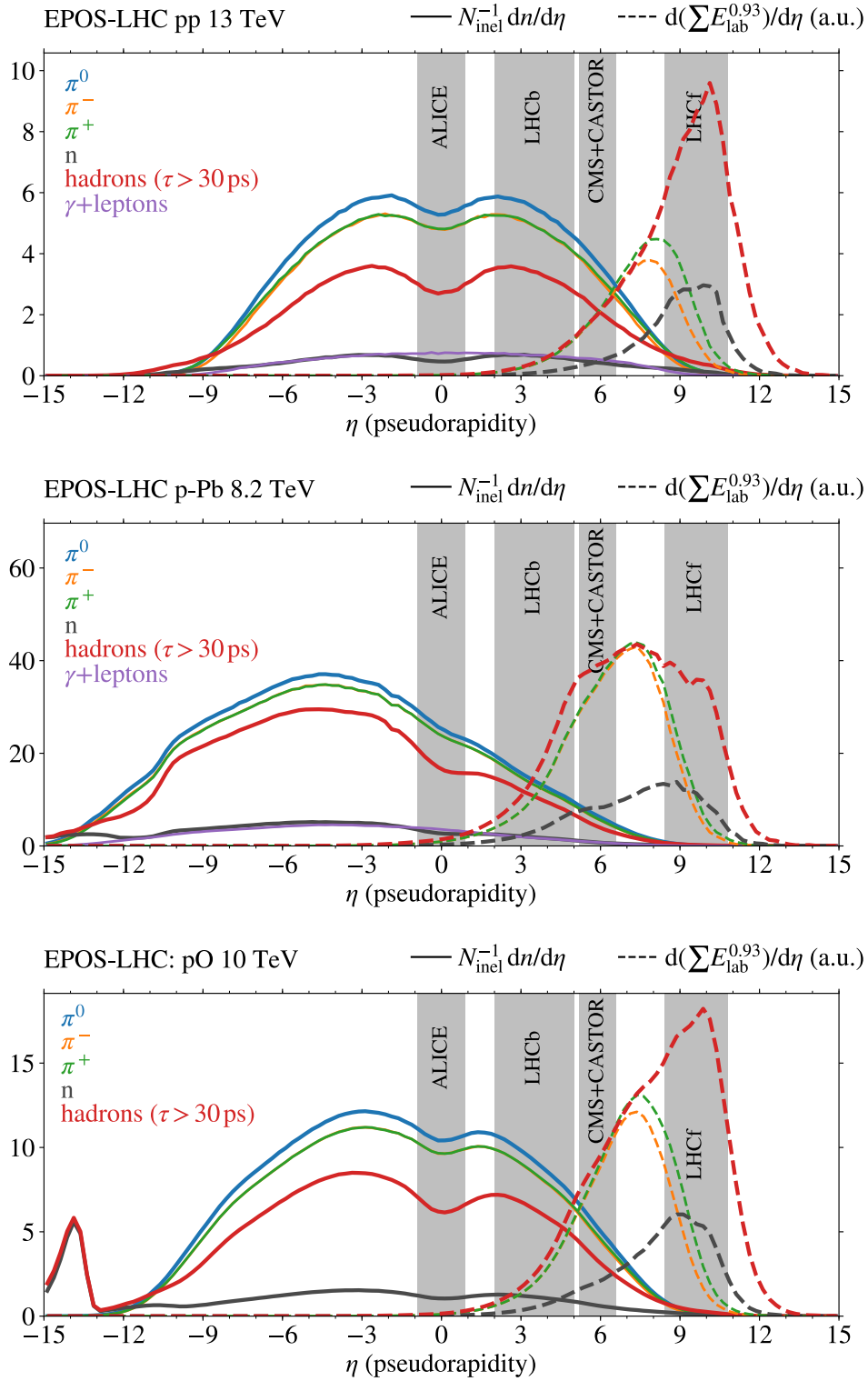


Figure 5: Simulated densities of prompt particles (solid lines) in high-energy p-p, p-Pb, and p-O collisions. Dashed lines show the estimated number of muons produced by the secondaries if they were propagated through the atmosphere, assuming $N_\mu \propto E_{lab}^{0.93}$, where E_{lab} is the energy of the secondaries in the boosted system. (Taken from [15])

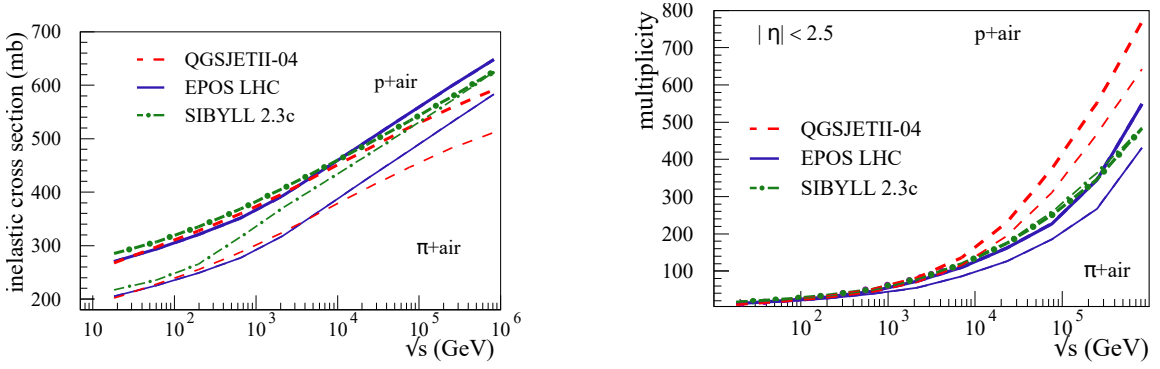


Figure 6: Inelastic cross sections (left) and multiplicity for $|\eta| < 2.5$ (right) for p-air (thick lines) and π -air (thin lines). (Taken from [24].)

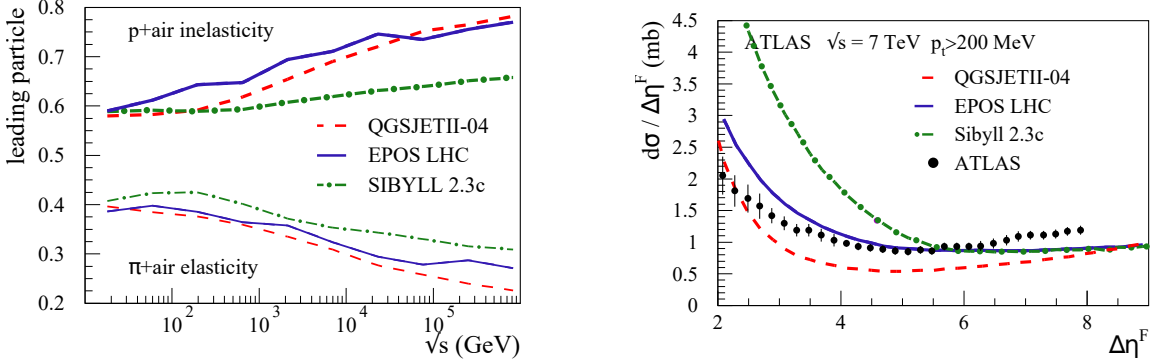


Figure 7: Left: Inelasticity in p-Air interactions (thick lines) and elasticity for π -Air interactions (thin lines). Right: ATLAS measurement of the pseudorapidity gap $\Delta\eta^F$ for particles with $p_{t,cut} > 200$ MeV in minimum bias events at 7 TeV. (Taken from [24].)

measurements, which also include data from IceCube [42], the Auger Underground Muon Detectors (UMD)[43], unpublished data from Yaktusk [44] and a new analysis of data from the AGASA experiment [45] was presented in [46].

A z -scale was introduced to plot the ratio of N_μ with respect to proton simulations with a given model, as

$$z = \frac{\ln N_\mu - \ln N_\mu^p}{\ln N_\mu^p - \ln N_\mu^{Fe}} \quad (3.1)$$

Where $z = 0$ corresponds to the number of muons contained in proton showers, and $z = 1$ in iron showers. An energy rescaling was applied to all z -values in order to obtain a matching energy spectrum between experiments. Figure 11 displays the compilation of all experiments with respect to different hadronic models, including those before the LHC. Afterwards, the difference with respect to expectations from models was calculated as $\Delta = z - z_{\text{mass}}$, where z_{mass} was inferred from a compilation of X_{max} data. Results are shown in Figure 12, where a growing muon deficit in the simulations can be observed above 10^{16} eV. The slope of this increase in z per decade in energy is 0.34 and 0.30 for EPOS-LHC and QGSJet-II.04 respectively, with 8σ significance.

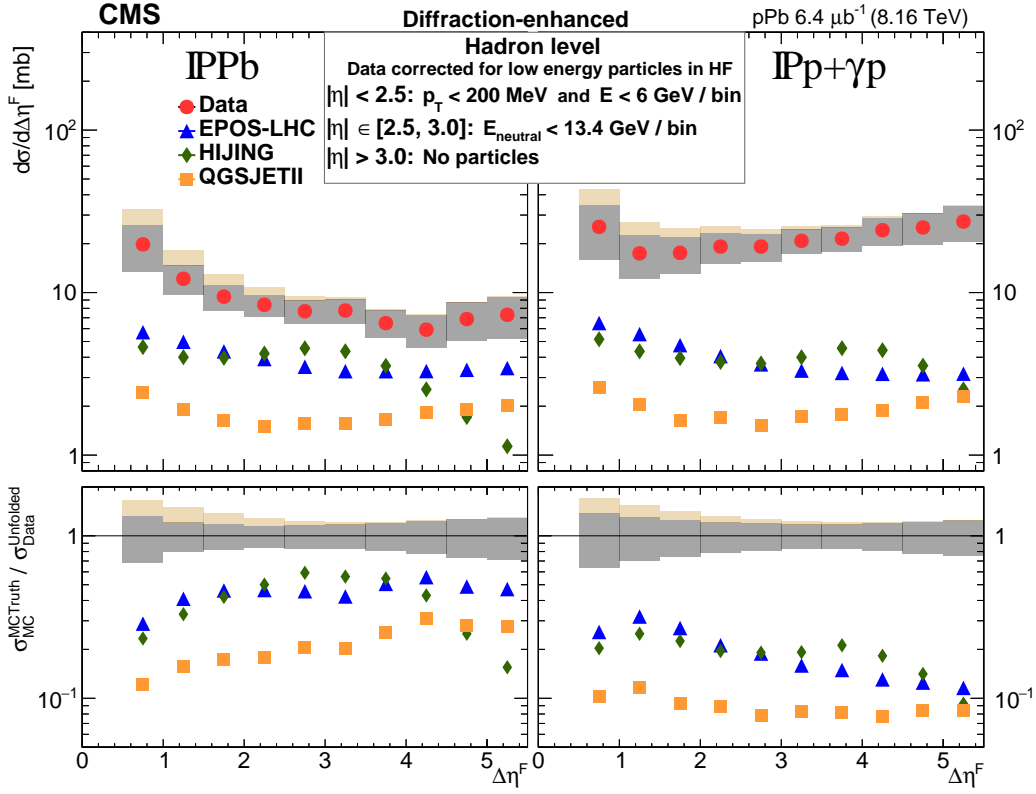


Figure 8: Unfolded diffraction-enhanced differential cross section $d\sigma/d\Delta\eta^F$ spectra compared to hadron level predictions of the EPOS-LHC, HIJING, and QGSJET II generators (taken from [26].)

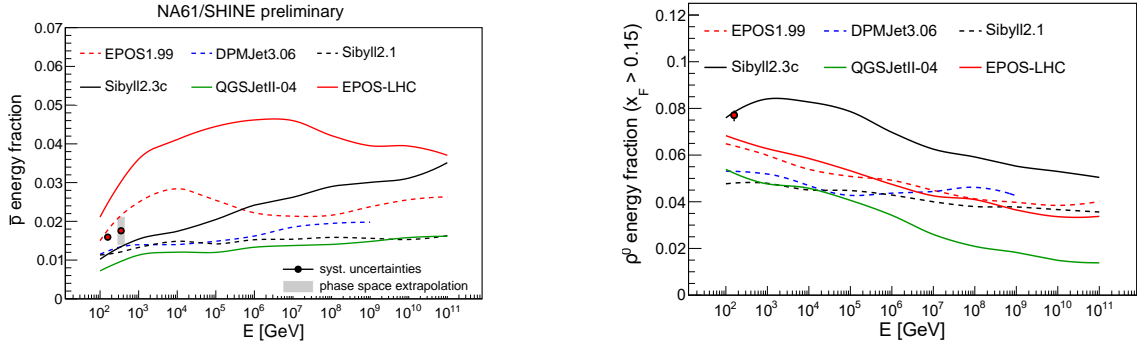


Figure 9: Energy fraction of anti-protons (left) and ρ^0 (right), as measured by NA61/SHINE in π^- -C interactions, and comparison with predictions from models. (Plot taken from [29].)

3.1 Muon energy and transverse momentum at production

In [47], the minimum energy required at production for a muon to be observed in each experiment ($E_{\mu\text{prod}}$) was calculated, ranging from roughly 1 GeV up to 19 GeV, as reported by NEVOD-DECOR [33, 34]. Unfortunately, due to the large inhomogeneity and uncertainties of measurements, no differences were found between simulations and data in the muon spectrum at

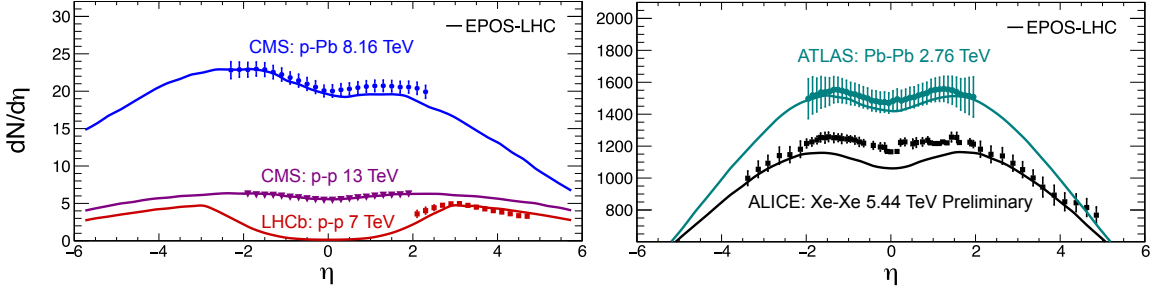


Figure 10: Comparison of $dN/d\eta$ measurements in different colliding systems with EPOS-LHC. (Taken from [31].)

production. However, the results from KASCADE-Grande’s findings at [48] indicate that the measured muon number falls between the predictions for proton and iron nuclei for all models, with a tendency towards heavier primaries as the EAS zenith angle increases. This suggests that there may be an issue with the predicted muon attenuation length between 10 PeV and 1 EeV.

Differences in the muon E-spectrum could potentially be caused by alterations in the π^\pm/K mix in the hadronic cascade, through the effective critical energy of the mix, or by discrepancies in the modelling of the E-spectra of π and K in the hadronic interactions. This was previously demonstrated in [12, 13] and Figure 3 (right). As a result, the E-spectrum of muons is an effective way to constrain hadronic physics. [49] studied the effects of shifts in the muon E-spectrum on different shower observables related to the distribution of muons at ground level. These effects are especially prominent at high zenith angles due to the energy threshold for muons imposed by the atmosphere. In addition, near the shower core, the variability of muon arrival times can be directly linked to their effective velocities [12].

Finally, so far, no evidences have been reported on deviations of the bulk of the p_t -distribution

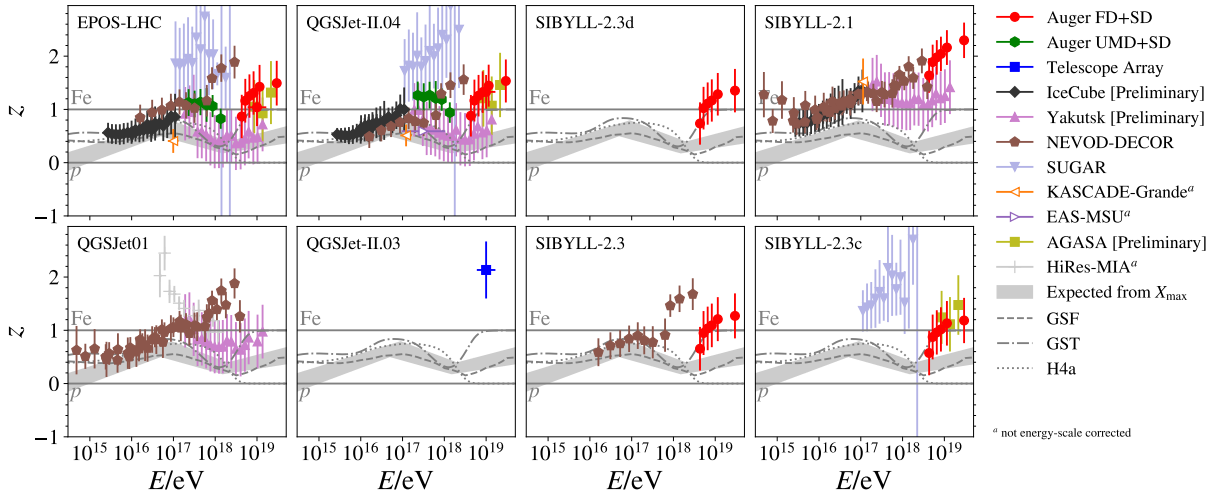


Figure 11: z-values from the latest WHISP compilation [46]. Shown for comparison are z-values expected for a mixed composition from optical measurements (X_{\max}), based on an update of Ref. [64], and from the flux models GSF [65], GST [66], and H4a [67].

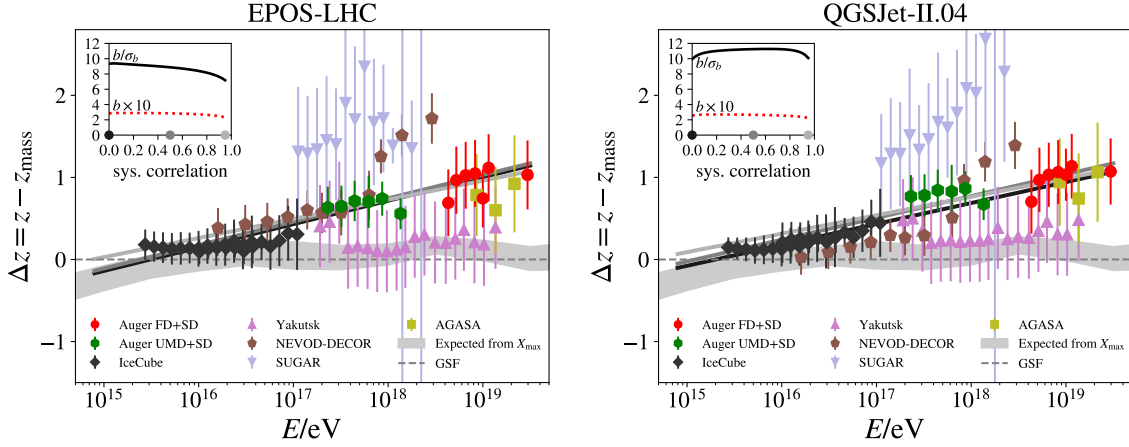


Figure 12: $\Delta z = z - z_{\text{mass}}$ for EPOS-LHC and QGSJet-II.04. The function $\Delta z_{\text{fit}} = a + b \log_{10}(E/10^{16} \text{eV})$ was fitted. The inset shows the slope, b , and its deviation from zero in standard deviations for an assumed correlation of the point-wise uncertainties within each experiment. Examples of the fits are shown for a correlation of 0.0, 0.5, and 0.95. (Taken from [46].)

of muons ²from the universal expectation.

3.2 Muon Production Depth

The MPD distribution of EAS enables us to track the longitudinal development of the hadronic cascade, particularly the depth at which mesons decay into muons. This depth is expected to reach its maximum (X_{max}^{μ}) around the point where the average energy of mesons is equal to the effective critical energy of the π^{\pm}/K mix. The longer the number of generations in the cascade, the deeper X_{max}^{μ} will be, meaning that it is sensitive to phenomena which can delay or accelerate the flow from the hadronic to the EM channel without changing the multiplicative process. This was investigated in [50] and [51] which looked at energies between 10^{15} and 10^{17} eV, and above $10^{19.2}$ eV respectively. The left of Figure 13 displays the $\langle X_{\text{max}}^{\mu} \rangle$ and $\langle X_{\text{max}} \rangle$ at $10^{19.4}$. These values showed tension with pre-LHC hadronic models for QGSJETII.04 and an extremely deep value of X_{max}^{μ} for EPOS-LHC, making it lie out of the p-Fe reach.

In [52], it was demonstrated that a considerable portion of the current discrepancies in model predictions of X_{max}^{μ} are caused by interactions between pions and air at very high energies, such as the inelastic cross sections and the production spectra of mesons and nucleons. Specifically, EPOS-LHC was found to have a deep X_{max}^{μ} due to an abundance of baryons produced by pion-air interactions at high energies, as well as a relatively high rate of inelastic diffraction in those collisions [53]. This was found to lead to a difference of $\Delta X_{\text{max}}^{\mu} \simeq 50 \text{ g cm}^{-2}$, which translates to a difference in the EM profile of $\Delta X_{\text{max}} \simeq 15 \text{ g cm}^{-2}$. The measurements of MPD provide a special chance to restrict the treatment of pion-air interactions at very high energies and to reduce the uncertainties in X_{max} that arise from models.

²More than 99% of muons are below $p_t < 2 \text{ GeV}/c$.

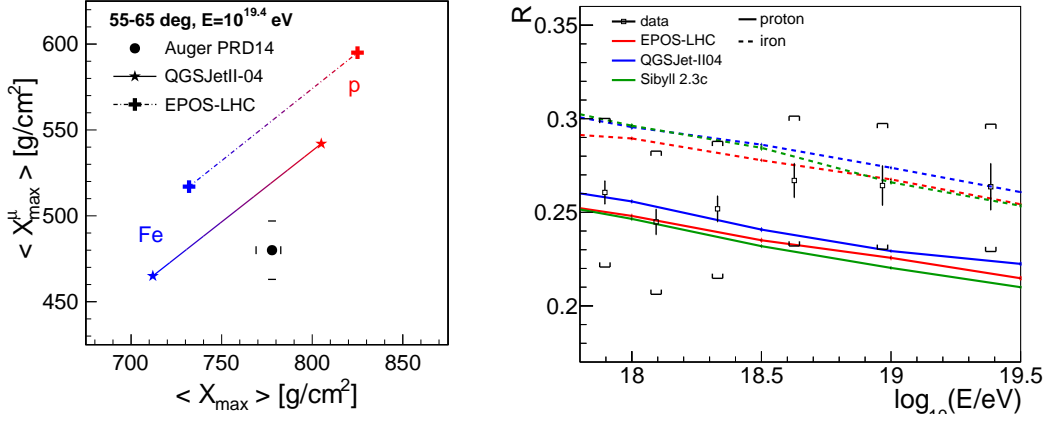


Figure 13: Left: Measurement of $\langle X_{\max}^{\mu} \rangle$ and $\langle X_{\max} \rangle$ for $10^{19.4}$ eV, with systematics uncertainties, as well as the phase-space (lines) occupied by EPOS-LHC and QGSJETII.04 models, extracted from [51]. Right: Parameter R of the average electromagnetic profile as a function of the EAS energy as measured by Auger, as well as predictions for different hadronic models, extracted from [54].

3.3 Electromagnetic Component

The traditional Gaisser-Hillas equation can be rewritten as

$$\frac{dE}{dX} = \left(1 + R \frac{X'}{L}\right)^{R-2} \exp\left(-\frac{X'}{RL}\right), \quad (3.2)$$

where $R = \sqrt{\lambda/|X'_0|}$, $L = \sqrt{|X'_0|\lambda}$ and $X'_0 = X_0 - X_{\max}$. This formulation is a Gaussian with standard deviation L multiplied by a term that introduces an asymmetry governed by R . The parameters R and L are less correlated than λ and X_0 . Furthermore, the parameter R is considered to be sensitive to the initiation of the electromagnetic shower, as it affects the rate of π^0 production, which consequently contributes to the EM shower. A recent study [54] has measured R , with the results being compatible with model expectations, although there are high systematic uncertainties involved. Therefore, it is difficult to draw any meaningful conclusions from the data.

4. Discussion

Attempts have been made to explain the muon problem by increasing the hadronic energy fraction of interactions f through different means such as the formation of a Strange Fireball [55], String Percolation [2], Chiral Symmetry Restoration [59], an increase in the inelastic cross section [60], or even Lorentz Invariance Violation [61] by effectively prolonging the lifetime of π^0 in order to keep them contributing to the hadronic cascade. It has been proposed that this deficit in N_{μ} with respect to expectations can be produced by small deviations δf accumulated along a number n of generations as $N_{\mu} \propto (f + \delta f)^n$. For example, a 5% deviation δf per generation, if it occurs over six generations, could result in a $\sim 30\%$ deviation. Alternatively, a larger single deviation from expectations ($\delta f \simeq 0.3 - 0.6$) could occur at the first generation, which is the farthest away from the reach of accelerator experiments and thus has less direct experimental constraints. This would

result in a change of the multi-particle production of the first interaction with energy, thus altering f_1 . The relation $\frac{d \ln N_\mu}{d \ln E} = \beta$ would then become $\frac{d \ln N_\mu}{d \ln E} = \frac{d \ln f_1}{d \ln E} + \beta$. A sudden change of f_1 would produce a change in the logarithmic slope. On the other hand, the continuous and smooth deviation of simulations with respect to data from low energies seen in Figure 12 suggests a small cumulative effect, generation after generation, rather than a sudden change.

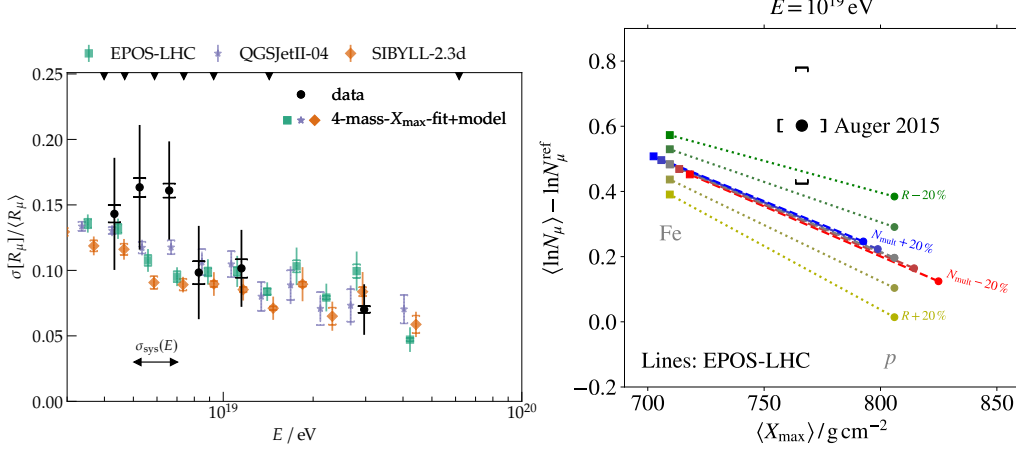


Figure 14: Left: Measurement of the fluctuation of the number of muons by Auger, compared to expectations from composition measurements (X_{\max}), taken from [38]. Right: Impact of changes of the hadron multiplicity $N_{\text{mult}} \equiv m$ (dashed lines) and the energy ratio $R \equiv \frac{f_{\text{EM}}}{f}$ (dotted lines) in collisions at the LHC energy of $\sqrt{s} = 13$ TeV on EPOS-LHC predictions for the air shower observables X_{\max} and $\langle \ln N_\mu \rangle$ in 10^{19} eV air showers. Data point is from Pierre Auger Observatory [36]. The model lines represent all CR-primary mixture from pure proton (bottom right) to pure iron (top left). The dashed and dotted lines represent modifications of N_{mult} and R in steps of 10% from their nominal values. (Taken from [57].)

In [56], a variable of the 1st interaction that combines the multiplicity and energy taken by the particles feeding the hadronic cascade was defined as

$$\alpha_1 = \sum_{j=1}^m (E_j/E_0)^\beta \quad (4.1)$$

where the index j runs over all particles contributing to the hadronic cascade and $\beta = 0.93$. The correlation of α_1 of the first interaction with the number of muons of the shower is 75%, whereas the correlation with f_1 is slightly smaller, 65%, due to the diffractive events. For most practical applications one can simply take $\alpha_1 \simeq f_1$. The relative fluctuations of N_μ can be expressed by a quadratic sum of the relative fluctuations of α_n in the different generations n

$$\left(\frac{\sigma(N_\mu)}{N_\mu} \right)^2 \simeq \left(\frac{\sigma(\alpha_1)}{\alpha_1} \right)^2 + \left(\frac{\sigma(\alpha_2)}{\alpha_2} \right)^2 + \dots + \left(\frac{\sigma(\alpha_c)}{\alpha_c} \right)^2 \quad (4.2)$$

where $\sigma(\alpha_n) \propto 1/\sqrt{m_1 \cdot m_2 \cdot \dots \cdot m_{n-1}}$, which decreases as the generation number gets higher. As a result the relative fluctuations of N_μ are dominated by the fluctuations of α_1 in the 1st interaction [56]. In p-Air interactions $\sim 70\%$ of the variance is due to the first interaction, whereas for nuclei of mass A , the fluctuations are reduced by a factor $\sim 1/\sqrt{A}$.

A similar process happens with the total signal of a photomultiplier. While the total gain is a result of the gain through all stages, the fluctuations of the final output are dominated by those within the 1st dynode [68, 69]. In this sense, fluctuations in the first stage (where the number of particles is still low) are propagated and amplified by later stages because the amplification factor becomes more stable as the number of participating electrons exponentially increases.

In [38], the Auger Collaboration measured the fluctuations of the number of muons as a function of the shower energy, which is displayed in Figure 14 (left), along with expectations from composition analysis. While interaction models accurately describe the relative fluctuations, they show a significant discrepancy compared to the average muon scale. These values, $\langle N_\mu \rangle$ and $\sigma(N_\mu)/\langle N_\mu \rangle$, depend on different aspects of the shower development. $\langle N_\mu \rangle$ is contributed to equally by all generations [1], while $\sigma(N_\mu)/\langle N_\mu \rangle$ is mainly impacted by the first interactions [56] through α_1 -fluctuations. Figure 14 (right), taken from [57], shows the influence of changing the ratio of electromagnetic to hadronic particles,

$$R \equiv \frac{f_{\text{EM}}}{f} = (f^{-1} - 1) \quad (4.3)$$

on the observables N_μ and X_{max} with a measurement from Auger [36], using the methodology described in [36]. While altering m (N_{mult}) results in the simulated line shifting parallel to itself, it is demonstrated that a modification of R affects N_μ and leaves X_{max} unchanged. It has been suggested that a decrease of R of 15% at the $\sqrt{13}$ TeV would be adequate to make simulations compatible with air shower data at 10^{19} eV. In [57], R was proposed as a possible experimental observable to be measured in LHC calorimeters as a function of pseudorapidity and central charged particle multiplicity. It is believed that its precision measurements to 5% at the LHC could potentially contribute to a better understanding of muon production in air showers [31], and even lead to distinguishing between quark-gluon-plasma-like (QGP-like) effects and alternative more microscopic effects.

5. Direct Measurement

The measurement of the p-Air cross sections by cosmic ray measurements is a unique case where one can directly access the properties of the first interaction. This is because p-Air interactions will produce a detectable deep tail on the X_{max} distributions, which is a direct mapping of the depth of the first interaction X_0 [62, 63]. Moreover, in [70], a method was proposed to measure the high energy end of the π^0 spectrum. This method is based on the fact that extreme low- N_μ fluctuations on p-Air interactions are visible if there are enough protons in the UHECR composition. The figure 15 shows the effect of changing the energy spectrum of π^0 in the first interaction (only), with its measurable effects on the extreme low- N_μ fluctuations of the p-Air interactions. This method provides a novel way to access the high energy end of the π^0 spectrum and a direct measurement of the properties of the first interaction.

6. Conclusions

Ultra High Energy Cosmic Rays offer a great prospect for furthering our understanding of particle physics, beyond the scope of what can be explored using accelerators. Our current comprehension of hadronic physics in the forward region and at the highest energies is merely an

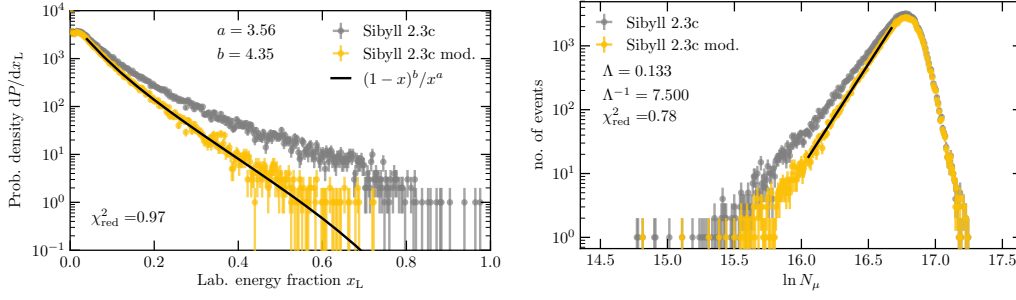


Figure 15: Left: Inclusive production cross-section of π^0 as a function of lab. energy for SIBYLL-2.3c [23]. A suppressed cross-section at large x_L is shown in yellow. Right: Distribution of the number of muons at ground level for the two production spectra shown in the figure on the left. (Taken from [70].)

extrapolation of what is known, making it vulnerable to inaccuracies. UHECR mass inference relies on EAS simulations that use high energy hadronic models, and this consequently brings the model uncertainties into the equation, thus posing a challenge to the quest to discover their origin.

LHC measurements have improved the agreement of models in explaining p-p collisions, however discrepancies still remain when it comes to p-Air and in particular π -Air collisions, which play a major role in the development of the EAS hadronic cascade. Consequently, new measurements for p-O are being proposed for the upcoming LHC phase, with the purpose of filling the gap with intermediate nuclei measurements at the highest energies.

Muon EAS observables, such as Muon Production Depth (MPD), the muon number, and the muon energy spectrum reveal some interesting facts. It has been demonstrated that the MPD results are remarkably sensitive to the modeling of diffractive π -Air interactions, which can indirectly reduce the X_{\max} model uncertainties. The energy spectrum of muons is sensitive to the energy spectrum of mesons, as well as the ratio of π /K mix of the hadronic cascade. Additionally, the muon deficit in simulations has been observed to begin around 10^{16} eV, with a steady and gradual trend. The shower-to-shower fluctuations of the muon number are mainly determined by the fluctuations of the partition of energy in the first interaction. The initial measured results of the muon number fluctuations around 10^{19} eV suggest a lack of significant divergence from expected results in the first UHECR-Air interactions. For this reason, the muon deficit is likely to result from the accumulation of small deviations throughout the various generations of the hadronic cascade, in *meson*-Air or nucleon-Air interactions. Several proposals have been made in order to increase the hadronic energy fraction ([58, 55, 60, 59]), which must be tested against the other EAS observables.

Finally, a measurement of the low tail of the muon number fluctuations has been suggested, as it is able to map the inclusive production π^0 cross-section in the first p-Air interaction, in a similar fashion to how the high X_{\max} -tail was employed to measure the p-Air cross section. This would be the first measurement of a multi-particle production characteristic beyond the 100 TeV scale.

Acknowledgments

I want to thank the Pierre Auger Collaboration, and in particular R. Riehn, R. Conceição and C. Dobrigkeit for proofreading and feedback on this manuscript. I want also to acknowledge the

financial support from Xunta de Galicia (Centro singular de investigación de Galicia accreditation 2019-2022), grant ED431F 2022/15 and ED431F 2022/15, by European Union ERDF, and by the “María de Maeztu” Units of Excellence program MDM-2016-0692 and the Spanish Research State Agency, grant PID2019-105544GB-I00 and program “Ramon y Cajal”, Grant No. RYC2019-027017-I.

References

- [1] J. Matthews, “A Heitler model of extensive air showers,” *Astropart. Phys.* **22**, 387 (2005)
- [2] J. Alvarez-Muniz, L. Cazon, R. Conceicao, J. D. de Deus, C. Pajares and M. Pimenta, “Muon production and string percolation effects in cosmic rays at the highest energies,” arXiv:1209.6474 [hep-ph].
- [3] L. Cazon, “Extensive Air Showers: from the muonic smoking guns to the hadronic backbone,” *EPJ Web Conf.* **52** (2013) 03003
- [4] M. Ave, R. Engel, M. Roth and A. Schulz, “A generalized description of the signal size in extensive air shower detectors and its applications,” *Astropart. Phys.* **87** (2017) 23.
- [5] M. Ave, M. Roth and A. Schulz, “A generalized description of the time dependent signals in extensive air shower detectors and its applications,” *Astropart. Phys.* **88** (2017) 46.
- [6] K. Greisen, The Extensive Air Showers. *Prog. in Cosmic Ray Physics*, III, 1 (1956)
- [7] T.K. Gaisser, A.M. Hillas. *Proc. of 15th Int. Cosmic Ray Conf.*, 13–26 Aug 1977. Vol. 8. Plovdiv, Bulgaria. p. 353.
- [8] A. Smialkowski and M. Giller, “Universality of electron distributions in extensive air showers,” *Astrophys. J.* **854** (2018) no.1, 48
- [9] M. Giller, A. Smialkowski and G. Wieczorek, “An extended universality of electron distributions in cosmic ray showers of high energies and its application,” *Astropart. Phys.* **60** (2015) 92
- [10] F. Nerling, J. Bluemer, R. Engel and M. Risse, “Universality of electron distributions in high-energy air showers: Description of Cherenkov light production,” *Astropart. Phys.* **24** (2006) 421
- [11] M. Giller, G. Wieczorek, A. Kacperczyk, H. Stojek and W. Tkaczyk, “Energy spectra of electrons in the extensive air showers of ultra-high energy,” *J. Phys. G* **30** (2004) 97.
- [12] L. Cazon, R. Conceicao, M. Pimenta and E. Santos, “A model for the transport of muons in extensive air showers,” *Astropart. Phys.* **36** (2012) 211
- [13] L. Cazon, R. Conceição and F. Riehn, “Universality of the muon component of extensive air showers,” [arXiv:2210.13407 [hep-ph]].
- [14] R. Ulrich *et al.* “Hadronic Multiparticle Production at Ultra-High Energies and Extensive Air Showers,” *Phys. Rev. D* **83** (2011) 054026
- [15] J. Albrecht, L. Cazon, H. Dembinski, A. Fedynitch, K. H. Kampert, T. Pierog, W. Rhode, D. Soldin, B. Spaan and R. Ulrich, *et al.* “The Muon Puzzle in cosmic-ray induced air showers and its connection to the Large Hadron Collider,” *Astrophys. Space Sci.* **367** (2022) no.3, 27
- [16] S. Ostapchenko, “On the re-summation of enhanced Pomeron diagrams,” *Phys. Lett. B* **636**, 40 (2006),
- [17] S. Ostapchenko, “Monte Carlo treatment of hadronic interactions in enhanced Pomeron scheme: QGSJET-II model,” *Phys. Rev. D* **83**, 014018 (2011),

- [18] S. Ostapchenko, "QGSJET-II: physics, recent improvements, and results for air showers," EPJ Web Conf. **52**, 02001 (2013)
- [19] T. Pierog, K. Werner, "EPOS Model and Ultra High Energy Cosmic Rays," Nucl. Phys. Proc. Suppl. **196**, 102 (2009),
- [20] T. Pierog, I. Karpenko, J.M. Katzy, E. Yatsenko, K. Werner, "EPOS LHC: Test of collective hadronization with data measured at the CERN Large Hadron Collider," Phys. Rev. C **92**, 034906 (2015),
- [21] E.J. Ahn, R. Engel, T.K. Gaisser, P. Lipari, T. Stanev, "Cosmic ray interaction event generator SIBYLL 2.1," Phys. Rev. D **80**, 094003 (2009),
- [22] F. Riehn, R. Engel, A. Fedynitch, T.K. Gaisser, T. Stanev, "A new version of the event generator Sibyll," PoS **ICRC2015** 558 (2015), 1510.00568 [PoS \(ICRC2015\) 558](#)
- [23] F. Riehn, H.P. Dembinski, R. Engel, A. Fedynitch, T.K. Gaisser, T. Stanev, PoS **ICRC2017**, 301 (2017), 1709.07227 [PoS \(ICRC2017\) 301](#)
- [24]
- [24] T. Pierog, "Hadronic Interactions and Air Showers: Where Do We Stand?," EPJ Web Conf. **208** (2019) 02002. doi:10.1051/epjconf/201920802002
- [25] D. d'Enterria and T. Pierog, "Global properties of proton-proton collisions at $\sqrt{s} = 100$ TeV," JHEP **1608** (2016) 170
- [26] [CMS], "First measurement of the forward rapidity gap distribution in pPb collisions at $\sqrt{s_{NN}} = 8.16$ TeV," [arXiv:2301.07630 [hep-ex]].
- [27] R. R. Prado [NA61/SHINE Collaboration], "Measurements of Hadron Production in Pion-Carbon Interactions with NA61/SHINE at the CERN SPS," [PoS \(ICRC2017\) 315](#)
- [28] A. Aduszkiewicz *et al.* [NA61/SHINE Collaboration], "Measurement of meson resonance production in $\pi^- + C$ interactions at SPS energies," Eur. Phys. J. C **77** (2017) no.9, 626
- [29] M. Unger [NA61/SHINE Collaboration], The Cosmic-Ray Program of the NA61/SHINE facility at the CERN SPS [PoS \(ICRC2019\) 446](#)
- [30] H. Dembinski, R. Ulrich and T. Pierog, "Future Proton-Oxygen Beam Collisions at the LHC for Air Shower Physics," [PoS \(ICRC2019\) 235](#)
- [31] Z. Citron *et al.*, "Future physics opportunities for high-density QCD at the LHC with heavy-ion and proton beams," arXiv:1812.06772 [hep-ph].
- [32] T. Abu-Zayyad *et al.* [MIA, HiRes Collaborations], "Evidence for Changing of Cosmic Ray Composition between 10^{17} -eV and 10^{18} -eV from Multicomponent Measurements," Phys. Rev. Lett. **84**, 4276 (2000),
- [33] A.G. Bogdanov, D.M. Gromushkin, R.P. Kokoulin, G. Mannocchi, A.A. Petrukhin, O. Saavedra, G. Trincherro, D.V. Chernov, V.V. Shutenko, I.I. Yashin, "Investigation of the properties of the flux and interaction of ultrahigh-energy cosmic rays by the method of local-muon-density spectra," Phys. Atom. Nucl. **73**, 1852 (2010).
- [34] A.G. Bogdanov, R.P. Kokoulin, G. Mannocchi, A.A. Petrukhin, O. Saavedra, V.V. Shutenko, G. Trincherro, I.I. Yashin, "Investigation of very high energy cosmic rays by means of inclined muon bundles," Astropart. Phys. **98** (2018), 13-20 Astropart. Phys. **98**, 13 (2018).

- [35] J.A. Bellido, R.W. Clay, N.N. Kalmykov, I.S. Karpikov, G.I. Rubtsov, S.V. Troitsky, J. Ulrichs, “Muon content of extensive air showers: comparison of the energy spectra obtained by the Sydney University Giant Air-shower Recorder and by the Pierre Auger Observatory,” *Phys. Rev.* **D98**, 023014 (2018),
- [36] A. Aab *et al.* [Pierre Auger Collaboration], “Muons in Air Showers at the Pierre Auger Observatory: Mean Number in Highly Inclined Events,” *Phys. Rev.* **D91**, 032003 (2015),
- [37] A. Aab *et al.* [Pierre Auger Collaboration], “Testing Hadronic Interactions at Ultrahigh Energies with Air Showers Measured by the Pierre Auger Observatory,” *Phys. Rev. Lett.* **117**, 192001 (2016),
- [38] A. Aab *et al.* [Pierre Auger], “Measurement of the Fluctuations in the Number of Muons in Extensive Air Showers with the Pierre Auger Observatory,” *Phys. Rev. Lett.* **126**, no.15, 152002 (2021) doi:10.1103/PhysRevLett.126.152002 [arXiv:2102.07797 [hep-ex]].
- [39] R.U. Abbasi *et al.* [Telescope Array Collaboration], *Phys. Rev.* **D98**, 022002 (2018),
- [40] W.D. Apel *et al.* [KASCADE-Grande Collaboration], *Astropart. Phys.* **95**, 25 (2017),
- [41] Yu.A. Fomin, N.N. Kalmykov, I.S. Karpikov, G.V. Kulikov, M.Yu. Kuznetsov, G.I. Rubtsov, V.P. Sulakov, S.V. Troitsky, *Astropart. Phys.* **92**, 1 (2017),
- [42] R. Abbasi *et al.* [(IceCube Collaboration)* and IceCube], “Density of GeV muons in air showers measured with IceTop,” *Phys. Rev. D* **106** (2022) no.3, 032010
- [43] A. Aab *et al.* [Pierre Auger], “Direct measurement of the muonic content of extensive air showers between 2×10^{17} and 2×10^{18} eV at the Pierre Auger Observatory,” *Eur. Phys. J. C* **80** (2020) no.8, 751 doi:10.1140/epjc/s10052-020-8055-y
- [44] A.V. Glushkov M.I. Pravdin, and A. Sabourov [Yakutsk Collaboration], private comm. (2018)
- [45] F. Gesualdi *et al.*, [PoS \(ICRC2021\) 473](#)
- [46] D. Soldin [EAS-MSU, IceCube, KASCADE-Grande, NEVOD-DECOR, Pierre Auger, SUGAR, Telescope Array and Yakutsk EAS Array], “Update on the Combined Analysis of Muon Measurements from Nine Air Shower Experiments,” [PoS \(ICRC2021\) 349](#)
- [47] L. Cazon, [EAS-MSU and IceCube and KASCADE-Grande and NEVOD-DECOR and Pierre Auger and SUGAR and Telescope Array and Yakutsk EAS Array Collaborations] [PoS \(ICRC2019\) 214](#)
- [48] J.C. Arteaga, [KASCADE-Grande Collaboration], [PoS \(ICRC2019\) 177](#)
- [49] J. Espadanal, L. Cazon and R. Conceição, “Sensitivity of EAS measurements to the energy spectrum of muons,” *Astropart. Phys.* **86** (2017) 32
- [50] W. D. Apel *et al.*, “Muon production height studies with the air shower experiment KASCADE-Grande,” *Astropart. Phys.* **34** (2011) 476.
- [51] A. Aab *et al.* [Pierre Auger Collaboration], “Muons in air showers at the Pierre Auger Observatory: Measurement of atmospheric production depth,” *Phys. Rev. D* **90** (2014) no.1, 012012
- [52] S. Ostapchenko, “High energy cosmic ray interactions and UHECR composition problem,” *EPJ Web Conf.* **210** (2019) 02001.
- [53] T. Pierog, “Open issues in hadronic interactions for air showers,” *EPJ Web Conf.* **145** (2017) 18002.
- [54] A. Aab *et al.* [Pierre Auger Collaboration], “Measurement of the average shape of longitudinal profiles of cosmic-ray air showers at the Pierre Auger Observatory,” *JCAP* **1903** (2019) no.03, 018
- [55] L. A. Anchordoqui, H. Goldberg and T. J. Weiler, “Strange fireball as an explanation of the muon excess in Auger data,” *Phys. Rev. D* **95** (2017) no.6, 063005

- [56] L. Cazon, R. Conceição and F. Riehn, “Probing the energy spectrum of hadrons in proton air interactions at ultrahigh energies through the fluctuations of the muon content of extensive air showers,” *Phys. Lett. B* **784** (2018) 68
- [57] S. Baur, H. Dembinski, T. Pierog, R. Ulrich and K. Werner, “The ratio of electromagnetic to hadronic energy in high energy hadron collisions as a probe for collective effects, and implications for the muon production in cosmic ray air showers,” arXiv:1902.09265 [hep-ph].
- [58] T. Pierog, S. Baur, H. Dembinski, R. Ulrich and K. Werner, “Collective Hadronization and Air Showers: Can LHC Data Solve the Muon Puzzle?,” *POS (ICRC2019)* 387
- [59] G. R. Farrar and J. D. Allen, “A new physical phenomenon in ultra-high energy collisions,” *EPJ Web Conf.* **53** (2013) 07007
- [60] G. R. Farrar, “Particle Physics at Ultrahigh Energies,” arXiv:1902.11271 [hep-ph].
- [61] R. Aloisio, D. Boncioli, A. di Matteo, P. L. Ghia, A. F. Grillo, S. Petrerá and F. Salamida, “Are Cosmic Rays still a valuable probe of Lorentz Invariance Violations in the Auger era?,” *Frascati Phys. Ser.* **58** (2014) 274
- [62] P. Abreu *et al.* [Pierre Auger Collaboration], “Measurement of the proton-air cross-section at $\sqrt{s} = 57$ TeV with the Pierre Auger Observatory,” *Phys. Rev. Lett.* **109** (2012) 062002
- [63] R. Ulrich [Pierre Auger Collaboration], “Extension of the measurement of the proton-air cross section with the Pierre Auger Observatory,” *POS (ICRC2015)* 401
- [64] K. H. Kampert and M. Unger, “Measurements of the Cosmic Ray Composition with Air Shower Experiments,” *Astropart. Phys.* **35** (2012), 660-678 doi:10.1016/j.astropartphys.2012.02.004 [arXiv:1201.0018 [astro-ph.HE]].
- [65] H. P. Dembinski *et al.* [IceCube], “Surface muons in IceTop,” *POS ICRC2015* (2016), 267 doi:10.22323/1.236.0267
- [66] T. K. Gaisser, T. Stanev and S. Tilav, “Cosmic Ray Energy Spectrum from Measurements of Air Showers,” *Front. Phys. (Beijing)* **8** (2013), 748-758 doi:10.1007/s11467-013-0319-7 [arXiv:1303.3565 [astro-ph.HE]].
- [67] T. K. Gaisser, “Spectrum of cosmic-ray nucleons, kaon production, and the atmospheric muon charge ratio,” *Astropart. Phys.* **35** (2012), 801-806 doi:10.1016/j.astropartphys.2012.02.010 [arXiv:1111.6675 [astro-ph.HE]].
- [68] J. R. Prescott, “A statistical model for photomultiplier single-electron statistics,” *Nuclear Instruments and Methods* **39** (1966) 173–179. doi:10.1016/0029-554X(66)90059-0.
- [69] H.H. Tan, "A STATISTICAL MODEL OF THE PHOTOMULTIPLIER GAIN PROCESS WITH APPLICATIONS TO OPTICAL PULSE DETECTION," *International Telemetering Conference Proceedings*, Volume 18 (1982) <http://hdl.handle.net/10150/612894>
- [70] L. Cazon, R. Conceição, M. A. Martins and F. Riehn, “Constraining the energy spectrum of neutral pions in ultra-high-energy proton-air interactions,” *Phys. Rev. D* **103** (2021) no.2, 022001 doi:10.1103/PhysRevD.103.022001 [arXiv:2006.11303 [astro-ph.HE]].